Behavioral/Systems/Cognitive

Multimodal Integration in Rostral Fastigial Nucleus Provides an Estimate of Body Movement

Jessica X. Brooks and Kathleen E. Cullen
Aerospace Medical Research Unit, Department of Physiology, McGill University, Montreal, Quebec H3G 1Y6, Canada

The ability to accurately control posture and perceive self-motion and spatial orientation requires knowledge of the motion of both the head and body. However, whereas the vestibular sensors and nuclei directly encode head motion, no sensors directly encode body motion. Instead, the convergence of vestibular and neck proprioceptive inputs during self-motion is generally believed to underlie the ability to compute body motion. Here, we provide evidence that the brain explicitly computes an internal estimate of body motion at the level of single cerebellar neurons. Neuronal responses were recorded from the rostral fastigial nucleus, the most medial of the deep cerebellar nuclei, during whole-body, body-under-head, and head-on-body rotations. We found that approximately half of the neurons encoded the motion of the body in space, whereas the other half encoded the motion of the head in space in a manner similar to neurons in the vestibular nuclei. Notably, neurons encoding body motion responded to both vestibular and proprioceptive stimulation (accordingly termed bimodal neurons). In contrast, neurons encoding head motion were sensitive only to vestibular inputs (accordingly termed unimodal neurons). Comparison of the proprioceptive and vestibular responses of bimodal neurons further revealed similar tuning in response to changes in head-on-body position. We propose that the similarity in nonlinear processing of vestibular and proprioceptive signals underlies the accurate computation of body motion. Furthermore, the same neurons that encode body motion (i.e., bimodal neurons) most likely encode vestibular signals in a body-referenced coordinate frame, since the integration of proprioceptive and vestibular information is required for both computations.

Introduction

The vestibular system has an essential role in everyday life; it contributes not only to the generation of reflexes but also to spatial perception and motor control. Because the vestibular receptor organs are located in the inner ear, they sense the motion of the head in space. However, the earliest stages of vestibular processing are characterized by the convergence of vestibular signals with information from multiple modalities. Notably, the integration of vestibular and proprioceptive information is vital for the accurate control of posture and balance as well as higher-order functions such as self-motion perception and spatial orientation. Neck proprioceptive inputs shape vestibulospinal reflexes so that the resultant corrective movements account for changes in the position of the head relative to the body (Tokita et al., 1989, 1991; Kennedy and Inglis, 2002). Additionally, the convergence of vestibular and neck proprioceptive inputs underlies the ability of human subjects to perceive body motion independently of head motion (Mergner et al., 1991).

Where are vestibular and neck proprioceptive cues integrated and how does the brain compute an estimate of body movement? Despite early vestibular–neck convergence in the vestibular system (Boyle and Pompeiano, 1981; Anastasopoulos and Mergner, 1982; Wilson et al., 1990), neurons in the vestibular nerve and nuclei of the rhesus monkey encode motion of the head, not body, during passive movements (Cullen et al., 2001; Cullen and Minor, 2002). At the next level of processing, the rostral fastigial nucleus (FN) of the cerebellum receives input from the vestibular nuclei and contributes to the generation of vestibulospinal reflexes. Whereas a subset of neurons in this nucleus encodes vestibular signals in a reference frame appropriate for estimating body motion (Kleine et al., 2004; Shaikh et al., 2004), whether these neurons encode motion of the body in space remains unknown.

A key question that remains is as follows: How does the brain compute an estimate of body motion relative to space? Here we addressed this question by comparing the responses of single rostral FN neurons to head versus body motion. We found that neurons could be divided into two classes: unimodal neurons, which responded exclusively to vestibular stimulation, and bimodal neurons, which responded to both vestibular and neck proprioceptor stimulation. Notably, unimodal neurons encoded motion of the head in space (i.e., similar to neurons in the vestibular nuclei), whereas bimodal neurons explicitly encoded motion of the body in space. Interestingly, bimodal neurons showed comparable tuning for the encoding of both sensory stimuli as a function of head position. This similarity is likely to underlie the ability of these neurons to robustly encode the motion of the body in space. Furthermore, we suggest that the neurons that encode body motion (i.e., bimodal neurons) are likely to be the same neurons that have been shown to encode vestibu-

Received April 23, 2009; revised July 13, 2009; accepted July 18, 2009.

This study was supported by the Canadian Institutes of Health Research and the Le Fonds québécois de la recherche sur la nature et les technologies. We thank M. Van Horn, M. Jamali, and D. Mitchell for critically reading this manuscript and S. Nuara and W. Kucharski for excellent technical assistance.

Correspondence should be addressed to Dr. Kathleen E. Cullen, Aerospace Medical Research Unit, 3655 Promenade Sir William Osler, Montreal, QC H3G 1Y6, Canada. E-mail: Kathleen.cullen@mcgill.ca.

DOI:10.1523/JNEUROSCI.1937-09.2009

 0270-6474/09/2910499-13$15.00/0

lar information in a body-referenced coordinate frame (Kleine et al., 2004; Shaikh et al., 2004), since the accurate encoding of body motion likely requires vestibular signals to be transformed from a head- to a body-centered reference frame.

Materials and Methods

Three rhesus monkeys (*Macaca mulatta*) were prepared for chronic extracellular recording using aseptic surgical techniques. All experimental protocols were approved by the McGill University Animal Care Committee and were in compliance with the guidelines of the Canadian Council on Animal Care.

Surgical procedures. The surgical techniques and anesthesia protocols were similar to those previously described by Roy and Cullen (2001). Briefly, under surgical levels of isoflurane (2–3% initially, and 0.8–1.5% for maintenance) an 18-mm-diameter eye coil (three loops of Teflon-coated stainless steel wire) was implanted in the eye behind the conjunctiva. In addition, a dental acrylic implant was fastened to the animal's skull using stainless steel screws. The implant held in place a stainless steel post used to restrain the animal's head, and a stainless steel recording chamber that was positioned to access the rostral FN (posterior and lateral angles of 28 and 30°, respectively). After the surgery, buprenorphine (0.01 mg/kg i.m.) was used for postoperative analgesia. Animals were given 2 weeks to recover from the surgery before any experiments were performed.

Data acquisition. During the experiments, the monkey sat comfortably in a primate chair, which was placed on a vestibular turntable. The chair was placed in the experimental apparatus so that the animal's head was centered within a 1 m^3 magnetic field coil system (CNC Engineering). With the monkey head restrained, extracellular single-unit activity was recorded using enamel-insulated tungsten microelectrodes (7–10 MΩ impedance; Frederick-Haer) as has been described previously (Roy and Cullen, 2001). The location of the rostral FN was determined relative to the abducens nucleus, which was identified based on its stereotypical discharge patterns during eye movements (Cullen and McCrea, 1993; Sylvestre and Cullen, 1999). Turntable velocity was measured using an angular velocity sensor (Watson Industries). Gaze, head, and body position were measured using the magnetic search coil technique as follows (Fuchs and Robinson, 1966; Judge et al., 1980): (1) gaze position was measured with the scleral coil that had been surgically implanted beneath the conjunctiva as described above; (2) head position was recorded using a second search coil that was securely fastened to the monkey's head implant; and (3) body position was measured using a third search coil, fixed to a primate jacket worn by the monkey (Lomir Biomedical) at the level of thoracic vertebra 7 (T7). Level T7 was chosen because it is well below the lowest level of neck muscle insertion (T3) and thus recordings would not be confounded by neck movements (McCluskey and Cullen, 2007). The location of T7 was verified by x ray and/or spinal palpation. During experiments, unit activity, horizontal gaze, head, body and target positions, and table velocity were recorded on digital audio tape for later playback. Action potentials were discriminated during playback using a windowing circuit (BAK) that was manually set to generate a pulse coincident with the rising phase of each action potential. Gaze, head, body, target position, and table velocity signals were low-pass filtered at 250 Hz (eight-pole Bessel filter) and sampled at 1000 Hz.

Behavioral paradigms. Using juice as a reward, monkeys were trained to follow a target light (HeNe laser) that was projected, via a system of two galvanometer-controlled mirrors, onto a cylindrical screen located 60 cm away from the monkey's head. Target, turntable motion, torque motor, and data displays were controlled on-line by a UNIX-based real-time data acquisition system (REX) (Hayes et al., 1982). Eye motion sensitivities to saccades and ocular fixation were characterized by having the head-restrained monkey attend to a target that stepped between horizontal positions over a range of ±30°. Neuronal responses were also recorded during smooth pursuit eye movements made to track sinusoidal target motion (0.5 Hz, 40°/s peak velocity). Neuronal sensitivities to passive head velocity were tested by rotating monkeys about an earth vertical axis (1 Hz, ±40°/s) in the dark (whole-body rotation) and while they suppressed their vestibulo-ocular reflex (VOR) by fixating a laser target that moved with the vestibular turntable (i.e., VOR cancellation condition).

After a neuron's response to eye and head motion had been characterized, we next investigated its sensitivity to neck proprioceptive inputs using four different approaches. First, the monkey's head was held stationary relative to the earth while its body was sinusoidally (1 Hz, ±40°/s) rotated below. This paradigm, termed "body-under-head rotation," was used to characterize neuronal responses to dynamic stimulation of neck proprioceptors. Second, the animal's head was rotated in 5° increments relative to its earth stationary body over a range of ±20°. The head was then held stationary for 1 s, and neuronal responses were measured to assess sensitivities to static changes in head-on-body position. Third, a torque motor (Kollmorgen) attached to the monkey's head was used to induce sinusoidal rotation of the head relative to a stationary body. This paradigm, termed "head-on-body rotation" resulted in stimulation of both proprioceptive and vestibular sensors. Last, during the whole-body rotation and body-under-head rotation paradigms described above, sinusoidal rotations were first applied with the head centered on the body (i.e., whole-body rotation) or the body rotated symmetrically about the zero head-on-body position (i.e., body-under-head rotation). Then, in a subset of neurons, testing was also done with the head initially oriented at different positions relative to the body to address whether there was an influence of static neck inputs on vestibular- and proprioceptor-induced modulation during whole-body and body-under-head rotations, respectively.

Analysis of neuronal discharges. Data were imported into the Matlab (The MathWorks) programming environment for analysis. Recorded gaze, head, and body position signals were digitally filtered with zero phase at 60 Hz using a 51st order finite-impulse-response filter with a Hamming window. Eye position was calculated from the difference between gaze and head position signals. Head-on-body position was calculated as the difference between head and body position. Gaze, eye, head, head-on-body, and body position signals were digitally differentiated to produce velocity signals. For each neurons' resting discharge, we computed the coefficient of variation (CV) (defined as the SD of the interspike interval/mean interspike interval) to obtain a measure of discharge regularity. Neural firing rate was represented using a spike density function in which a Gaussian was convolved with the spike train (SD of 10 ms) (Cullen et al., 1996). Statistical significance was determined using paired Student's *t* tests.

In this study, we present data only from neurons that were sensitive to passive whole-body rotations but were not sensitive to eye motion. To verify that a neuron was unresponsive to eye position and/or velocity, we analyzed periods of steady fixation and saccade-free smooth pursuit using a multiple regression analysis (Roy and Cullen, 1998, 2001). In addition, spike trains were assessed to confirm that neurons neither paused nor burst during saccades.

A least-squares regression analysis was then used to describe each unit's response to vestibular stimulation during whole-body rotations as follows:

$$\hat{fr}(t) = b + S_{\text{v-vest}}\dot{H}(t) + S_{\text{a-vest}}\ddot{H}(t), \quad (1)$$

where $\hat{fr}(t)$ is the estimated firing rate, $S_{\text{v-vest}}$ and $S_{\text{a-vest}}$ are coefficients representing sensitivities to head velocity and acceleration, b is a bias term, and $\dot{H}(t)$ and $\ddot{H}(t)$ are head velocity and head acceleration, respectively. The estimated coefficients $S_{\text{v-vest}}$ and $S_{\text{a-vest}}$ were then used (Sadeghi et al., 2009) to calculate each unit's sensitivity [(sp/s)/(°/s)] and phase shift (°) relative to head velocity. Notably, a similar approach was used in the analysis of responses recorded during both whole-body rotation in the dark and VOR cancellation, thereby providing two estimates of a neuron's head velocity sensitivity.

A comparable approach was next used to describe each unit's response to proprioceptive stimulation during passive rotation of the body under a stationary head using the following equation:

$$\hat{fr}(t) = b + S_{\text{v-neck}}\dot{B}(t) + S_{\text{a-neck}}\ddot{B}(t), \quad (2)$$

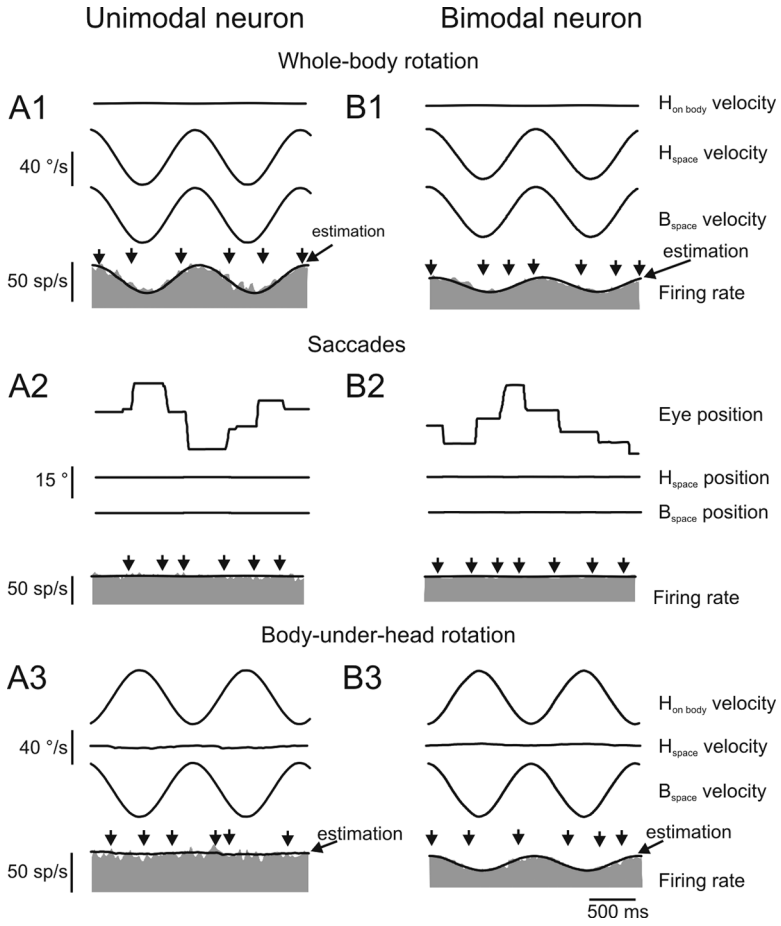

Figure 1. Characterization of rostral FN neuron types. Activity of example unimodal (left) and bimodal (right) neurons during basic paradigms. ***A1***, ***B1***, Neurons were identified by their response to horizontal head rotation during whole-body rotations. ***A2***, ***B2***, Static eye position sensitivity was studied by having the animal fixate laser targets moved in 5° steps. Only segments in which neither the head nor the eye moved were used for this analysis. ***A3***, ***B3***, Neck proprioceptor stimulation was applied by rotating the body under the head. Note that unimodal neurons are not modulated during this paradigm, whereas bimodal neurons show robust responses. Thick lines overlaying the firing rate represent a model based on estimated resting discharge and head (***A1***, ***B1***) or body (***A3***, ***B3***) velocity sensitivities. Vertical arrows show times that saccades occurred to highlight that there was no change in activity during vestibular quick phases.

where $\hat{fr}(t)$ is the estimated firing rate, $S_{\text{v-neck}}$ and $S_{\text{a-neck}}$ are coefficients representing sensitivities to body velocity and acceleration, and $\dot{B}(t)$ and $\ddot{B}(t)$ are body velocity and acceleration, respectively. Note that because neuronal responses typically led rather than lagged body velocity, our formalization of the model included velocity and acceleration terms. However, responses could have been equivalently well fit by a model formulation characterized by velocity and position terms, since position and acceleration terms are effectively redundant in the analysis of sinusoidal responses.

Finally, we described each unit's response during combined vestibular and proprioceptive stimulation evoked by head-on-body rotations (i.e., the combined condition) using the following equation:

$$\hat{fr}(t) = \text{b} + (S_{\text{v-vest}} + S_{\text{v-neck}})\,\dot{HB}(t) + (S_{\text{a-vest}} + S_{\text{a-neck}})\,\ddot{HB}(t), \tag{3}$$

where $\dot{HB}(t)$ and $\ddot{HB}(t)$ are head-on-body velocity and acceleration, respectively, and $\dot{HB}(t)$ is defined as $\dot{H}(t) - \dot{B}(t)$. Note that in this condition, neck proprioceptive and vestibular sensitivities could not be dissociated and thus were estimated as a single coefficient. Estimated sensitivities were then compared with those predicted based on the vestibular and proprioceptive sensitivities estimated for the same neuron during whole-body rotations (Eq. 1) and body-under-head rotations (Eq. 2), respectively. This prediction was termed the "summation model," since it was based on the sum of vestibular and neck sensitivities measured when each stimulus was delivered separately. We compared the ability of the summation model and a model based solely on the neuron's response to vestibular stimulation (i.e., Eq. 1, termed the "vestibular model") to describe neuronal responses during combined stimulation.

To quantify the ability of the linear regression analysis to model neuronal discharges, the variance-accounted-for (VAF) provided by each regression equation was determined. The VAF was computed as $\{\text{VAF} = 1 - [\text{var}(\hat{fr} - \text{fr})/\text{var}(\text{fr})]\}$, where $\hat{fr}$ represents the modeled firing rate (i.e., regression equation estimate), fr represents the actual firing rate, and var represents variance. Values are expressed as mean ± SEM and Student's *t* tests were used to determine whether the average of two measured parameters differed significantly from each other. Note that only data for which the firing rate was >20 sp/s were included in the optimization.

To determine whether each individual cell was better fit with the vestibular or summation model linear regression analyses were used to fit both models. To evaluate how well these models fit the data we used a partial correlation analysis. To remove the influence of correlations between the predictions themselves, we calculated partial correlation coefficients R_{v} (vestibular model) and R_{s} (summation model) using the following formulas:

$$R_{\text{v}} = \frac{(r_{\text{v}} - r_{\text{s}}r_{\text{sv}})}{\sqrt{(1 - r_{\text{s}}^2)(1 - r_{\text{sv}}^2)}} \tag{4}$$

and

$$R_{\text{S}} = \frac{(r_{\text{s}} - r_{\text{v}}r_{\text{sv}})}{\sqrt{(1 - r_{\text{v}}^2)(1 - r_{\text{sv}}^2)}}, \tag{5}$$

where r_{v} and r_{s} are the simple correlation coefficients (equivalent to the square root of VAF from equation 1 and 3) between the data obtained and each of the model predictions and r_{sv} describes the correlation between the two models. Partial correlation coefficients were then converted to *z* scores using Fisher's *r*-to-*z* transform to facilitate the comparison between the two models (Angelaki et al., 2004; Smith et al., 2005). The advantage of this comparison is that when *z* scores for one model are plotted versus the respective *z* scores for the other model, the plot can be easily separated into regions better fit by either model or equally well fit by both models.

Finally, tuning curves for different head-on-body positions were fit with Gaussian curves with the following equation:

$$\text{Sensitivity} = Ae^{\frac{-(\text{position}-\mu)^2}{2\sigma^2}}, \tag{6}$$

where μ represents the mean, σ (SD of the curve) is a measure of the width, and A is the amplitude from the peak to base of the Gaussian curve.

Results

Each of the neurons in our sample ($n = 83$) were modulated in response to vestibular stimulation and were insensitive to eye movements consistent with vestibular-only neurons previously described in the rostral FN and vestibular nucleus [rostral FN: Gardner and Fuchs (1975), Shaikh et al. (2005); vestibular nu-

cleus: Scudder and Fuchs (1992), Cullen and McCrea (1993), McCrea et al. (1999), Roy and Cullen (2004)]. First, as is illustrated in Figure 1, top, neurons robustly encoded vestibular information during sinusoidal yaw rotations about an earth vertical axis (Fig. 1*A1*,*B1*) [$S_{v\text{-}vest}$ 0.55 and 0.41(sp/s)/(°/s), respectively, for the two example neurons]. Because passive rotation elicited a compensatory eye motion response (i.e., the VOR), neuronal responses were also characterized during whole-body rotation while the monkey suppressed its VOR by fixating a visual target that moved with its head. The head velocity sensitivities of the two representative neurons in Figure 1 were comparable during rotation in darkness and in the VOR cancellation condition ($p = 0.53$ for our population). Depending on whether a neuron's firing rate increased during ipsilaterally (Fig. 1*A1*,*B1*) ($n = 32$) or contralaterally ($n = 31$) directed whole-body rotation, neurons were classified as type I or type II, respectively. In addition, all neurons were unresponsive to eye position during ocular fixation and saccades (Fig. 1*A2*,*B2*), pursuit (data not shown), and the quick phases of vestibular nystagmus (Fig. 1*A1*,*B1*, arrows).

Fastigial neurons are modulated by proprioceptive as well as vestibular stimulation

We next addressed whether the same rostral FN neurons that respond to vestibular stimulation also respond to the activation of neck proprioceptors. Several recent studies in alert rhesus monkeys have shown that changes in static neck position can influence the peak response modulation of these same neurons for a given vestibular stimulus (Kleine et al., 2004; Shaikh et al., 2004). Although these results have led to the proposal that the integration of neck proprioceptive and vestibular inputs underlies the observed neck-position dependent gain changes, the hypothesis had not been explored. To explicitly test this proposal, we recorded neuronal activities during a paradigm in which neck proprioceptor stimulation was delivered in isolation. The bottom rows of Figure 1 illustrate the responses recorded from the two example neurons while we sinusoidally rotated the monkey's body beneath its earth-stationary head. The majority of neurons ($n = 63$) remained sufficiently well isolated during this condition, allowing us to quantify their responses. Of these, ~50% ($n = 32$) were insensitive to neck proprioceptor stimulation (Fig. 1*A3*), whereas the remaining half ($n = 31$) showed significant modulation (Fig. 1*B3*) [$S_{v\text{-}neck} = 0.40$ (sp/s)/(°/s)]. Accordingly, based on their responses during vestibular stimulation (i.e., whole-body rotations) and neck proprioceptive stimulation (i.e., body-under-head rotations), neurons were categorized as either unimodal (responding only to vestibular stimulation) (Fig. 1, left) or bimodal (responding to both vestibular and neck proprioceptive stimulation) (Fig. 1, right).

Figure 2 summarizes the population data for both groups of neurons. Figure 2, *A* and *B*, shows the distributions of neuronal neck and vestibular sensitivities, respectively. During body-under-head rotation, the response modulation of bimodal neurons slightly led neck velocity (mean phase = 15.0 ± 37°) with a mean $S_{v\text{-}neck}$ of 0.34 ± 0.19 (sp/s)/(°/s). As expected, the average modulation of unimodal neurons was not significantly different from zero (Fig. 2*A*) ($p = 0.22$). In contrast, the vestibular sensitivities of both groups of neurons were comparable (Fig. 2*B*) [$S_{v\text{-}vest}$ 0.39 ± 0.11 vs 0.36 ± 0.13 (sp/s)/(°/s) for bimodal and unimodal cells, respectively; $p = 0.63$], as were average response phases relative to rotational velocity (5 ± 19° vs 15 ± 21°; $p = 0.29$, respectively). Each neuron's CV of the interspike interval (Fig. 2*C*) (see Materials and Methods) and resting discharge (Fig. 2*D*) were also determined in the absence of vestibular or neck

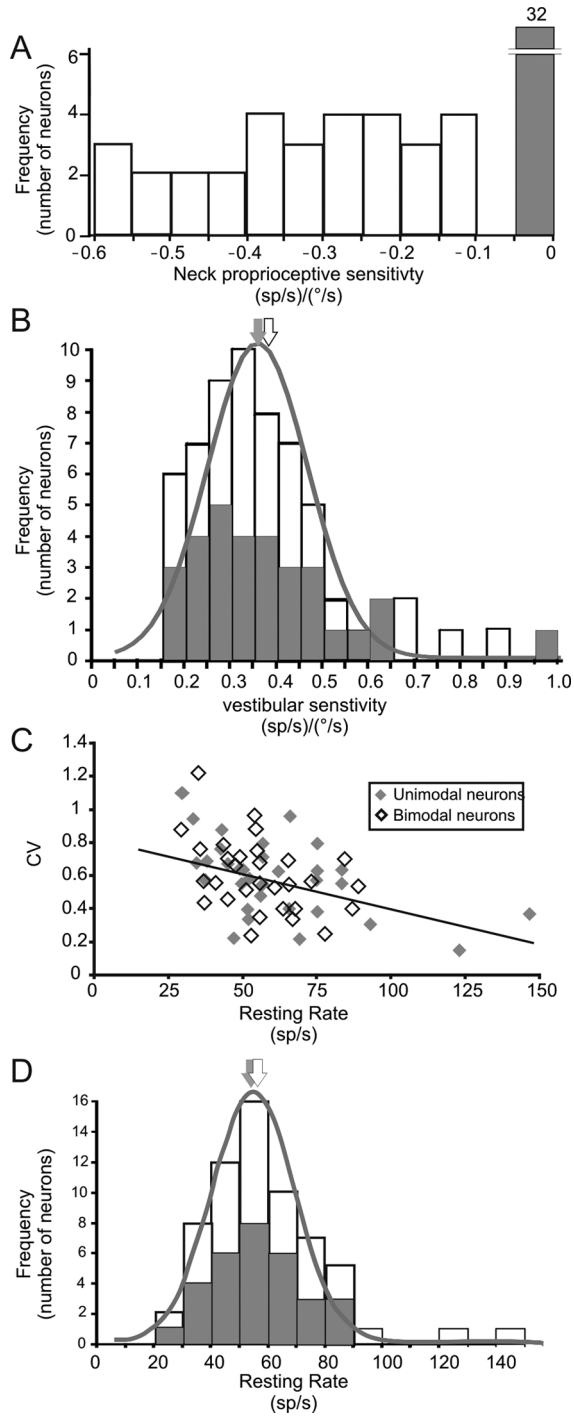

Figure 2. Distribution of neck proprioceptive and vestibular sensitivities and basic discharge parameters of rostral FN neurons. ***A***, Distribution of neck proprioceptive sensitivities. Classification of neurons was done according to the sensitivity of their discharge to body-under-head rotation. Cells with no neck proprioception sensitivity [i.e., <0.1 (sp/s)/(°/s)] were classified as unimodal neurons ($n = 32$), whereas cells with a proprioception sensitivity >0.1 (sp/s)/(°/s) were classified as bimodal neurons ($n = 31$). ***B***, Distribution of vestibular sensitivities determined during whole-body rotation. Gray and white arrows indicate the mean values for unimodal and bimodal neurons, respectively. ***C***, Relationship between the coefficient of variation and the resting rate of unimodal neurons (filled diamonds) and bimodal neurons (empty diamonds). ***D***, Distribution of resting discharge rate for the entire population. Gray and white arrows indicate the mean values for unimodal and bimodal neurons, respectively. All curves are fits for the whole neuronal population.

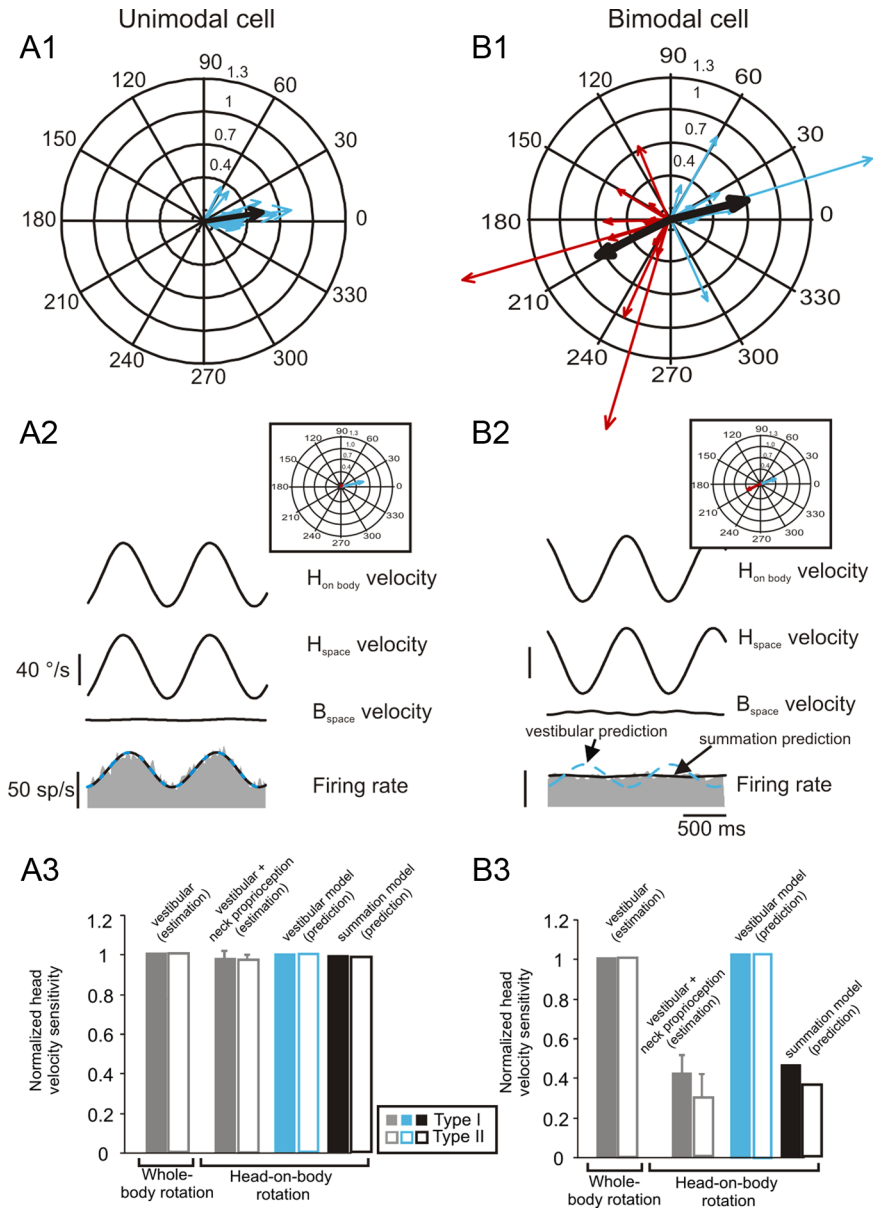

Figure 3. Combined vestibular–neck proprioceptive stimulation. Top, Polar plots of the vestibular (blue) and neck proprioceptive (red) sensitivities of unimodal (***A1***; $n = 15$) and bimodal (***B1***; $n = 13$) neurons, respectively. The length of the arrows indicates the sensitivity, and the angle represents the phase of the response. Superimposed black arrows are mean population vectors for vestibular and neck proprioceptive stimulation. Middle, Activity of example neurons (Fig. 1) during head-on-body rotations. Note that the unimodal neuron's activity (***A2***) could be predicted based on a summation of their neck proprioceptor and vestibular sensitivity (black line) or by its vestibular sensitivity alone (dashed blue line). In contrast, the modulation of the bimodal neuron (***B2***) was not well predicted based solely on its vestibular sensitivity (dashed blue line) but rather was better modeled by a prediction based on both its vestibular and neck proprioceptive sensitivities [black line; summation model (see Materials and Methods)]. Insets show polar plots of the vestibular and neck sensitivities as in ***A1*** and ***B1*** for the example neurons. Bottom, Histogram comparing sensitivities to vestibular and combined stimulation of type I (gray filled bars) and type II (gray empty bars) unimodal (***A3***) and bimodal (***B3***) neurons normalized to whole-body rotation sensitivity. For comparison, the predictions of the summation (black) and vestibular (blue) models are shown. Error bars represent ±SE.

stimulation with the animal's head centered on its body. On average, the resting discharges of unimodal and bimodal neurons were comparable (unimodal: 54 ± 19 sp/s; bimodal: 57 ± 16 sp/s; $p = 0.51$). Moreover, there was no difference in the resting discharge regularity (CV) of unimodal versus bimodal neurons ($p = 0.52$) (Fig. 2*C*), and the responses of unimodal neurons remained unchanged from resting values during neck proprioceptor stimulation ($p = 0.13$). Reconstruction of the recording sites showed that the locations of unimodal and bimodal neurons overlapped completely; there was no evidence of separate neuron clusters, and it was not uncommon to record both neuron types on the same track. Comparison of the responses of type I and type II neurons revealed that resting discharge rates, discharge regularities, and neck and vestibular sensitivities were comparable for both unimodal and bimodal neurons. Accordingly, for the purpose of this paper, we consider types I and II of each group collectively, since they encoded similar signals during each condition; the only difference was the direction of their modulation.

Fastigial neuron responses to simultaneous proprioceptive and vestibular stimulation

Whenever we turn our head on our body, vestibular sensors and neck proprioceptors are simultaneously activated. Accordingly, we next addressed the question of how vestibular and neck proprioceptive information would be integrated at the level of individual neurons in everyday life where inputs are not delivered in isolation. Prior studies in decerebrate animals had suggested that during combined stimulation, central neurons encode the sum of vestibular and proprioceptive responses measured when each stimulus is delivered separately [e.g., cat vestibular nucleus: Boyle and Pompeiano (1981), Anastasopoulos and Mergner (1982); and cat rostral FN: Stanojević (1981)]. To directly test whether these inputs sum linearly in alert monkeys, we first computed the vestibular and proprioceptive response vectors for our populations of unimodal and bimodal neurons. The vector was computed based on the gain (length) and phase (angle) of the neural responses to each stimulus. The polar plots in Figure 3, *A1* and *B1*, show response gains and phases for each group of neurons. The blue arrows represent neuronal responses measured when vestibular stimuli were applied in isolation (Fig. 1*A1*,*B1*), whereas the red arrows represent neuronal responses measured when proprioceptive stimuli were applied in isolation (Fig. 1*A3*,*B3*). Note that neck movement sensitivity vectors were not associated with unimodal neurons, since these neurons were insensitive to neck rotations [$S_{v\text{-}neck} < 0.1$(sp/s)/(°/s)]. Superimposed on each polar plot are the average vestibular and proprioceptive response vectors (corresponding superimposed black arrows), computed from the sum of the individual vestibular and proprioceptive response vectors. The lengths and directions of average vestibular response vectors were comparable for both groups of neurons (Fig. 3*A1*,*B1*, compare thick arrows; length $p = 0.21$, direction $p = 0.12$). Moreover, the lengths of average vestibular

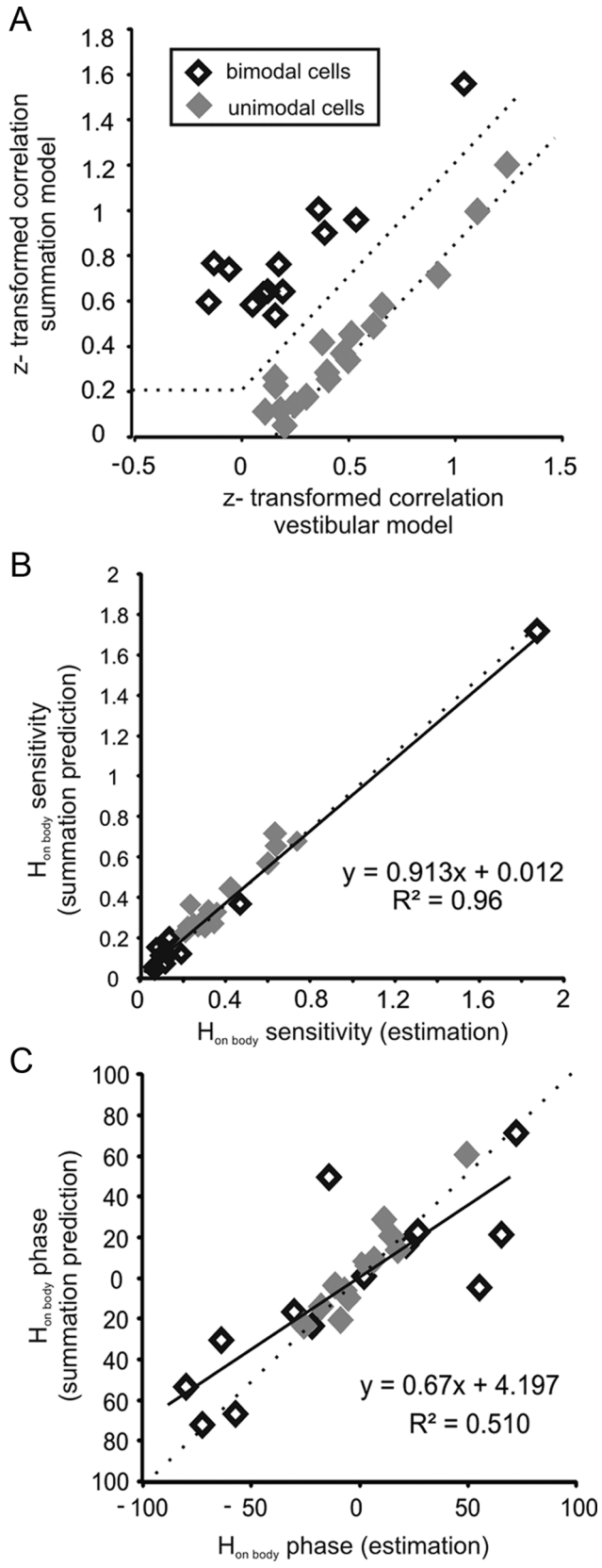

Figure 4. Predicting head-on-body responses based on responses during whole-body and body-under-head rotations. ***A***, Scatter plots of *z* scores corresponding to the partial correlation coefficients for fits of each neuron's response with the vestibular and summation models ($n = 28$). The superimposed dashed lines show three regions: the upper left area corresponds to responses that were significantly better fit by the summation model, the lower right area includes neurons that were significantly better fit by the vestibular model, and an in-between area includes cells that were not significantly better fit by either model. ***B***, Comparison of estimated and predicted sensitivities of unimodal (filled diamonds) and bimodal (empty diamonds) neurons to head-on-body rotations. The linear addition of vestibular and neck proprioceptor sensitivities provided a good prediction of each neuron's modulation during this paradigm. ***C***, Comparison of the estimated and predicted phase of the response of unimodal and bimodal neurons during head-on-body rotations. Dotted lines are the unity line and the solid lines are the regression lines (***B*** and ***C***) fit through all data points.

and proprioceptive response vectors were comparable for our sample of bimodal cells (Fig. 3*B1*, compare thick arrows; $p = 0.66$). Notably, bimodal neurons consistently had vestibular and neck proprioceptive responses that were antagonistic (Fig. 3*B1*, compare phase of arrows). As a result, during head-on-body motion the vestibular and neck proprioceptive sensitivities effectively cancelled each other and the resulting modulation was minimal. Accordingly, our convention was to define $S_{v\text{-}neck}$ negative relative to $S_{v\text{-}vest}$.

If our initial hypothesis was correct, the oppositely modulated inputs from neck proprioceptors should effectively suppress the vestibularly driven responses of bimodal neurons when head movements are made by turning the neck. To test this proposal, we next recorded the response of the same neurons while the head was rotated so that it moved relative to an earth-stationary body (i.e., head-on-body rotations). The responses of the two example neurons (the same neurons in Fig. 1) are shown in Figure 3, *A2* and *B2*. The insets show the vestibular and proprioceptor response vectors for each example neuron when the two stimuli were applied in isolation. The example neurons are typical in that their modulation could be predicted by the linear summation of the response vectors. Specifically, the example unimodal neuron (Fig. 3*A2*) responded robustly with a gain and phase that was not different from that measured during pure vestibular stimulation. In contrast, for the same head-in-space rotation, the modulation of the example bimodal neuron (Fig. 3*B2*) was greatly attenuated when the head was rotated on the body compared with when the head and body were rotated together in space (vestibular model; blue dashed line). Notably, this absence of robust modulation could be predicted based on the sum of the neuron's vestibular and proprioception sensitivity measured when each stimulus was delivered separately (summation model; solid black line).

Figure 3, *A3* and *B3*, shows average response gains (gray filled and empty bars; normalized relative to those measured during the vestibular-only stimulation condition) for both populations of cells. Response gains (Fig. 3*A3*) and phases were comparable for unimodal neurons during passive head-on-body rotations and vestibular-only stimulation (gain: $p = 0.58$; phase: $p = 0.41$). In response to the same head-in-space motion stimuli, however, the modulation of the bimodal neuron population was significantly (62%; $p < 0.05$) reduced compared with that observed for the same neurons during vestibular-only stimulation (Fig. 3*B3*), and response phases also differed significantly in the two conditions (5 versus −12°; $p < 0.05$). For all cells, the summation of neuronal sensitivities to head and neck rotation when applied alone predicted responses to head-on-body rotations; estimated and predicted sensitivities were not significantly different (Eq. 3; $p = 0.57$). Accordingly, unlike unimodal cells, a vestibular-based model could not predict the responses of bimodal neurons during combined stimulation; estimated and predicted sensitivities were significantly different (Eq. 1; $p < 0.05$).

The results shown in Figure 3 were further quantified by computing an *r*-to-*z* transform of the partial correlation coefficients of these two models. Figure 4*A* plots the *z*-transformed partial

←

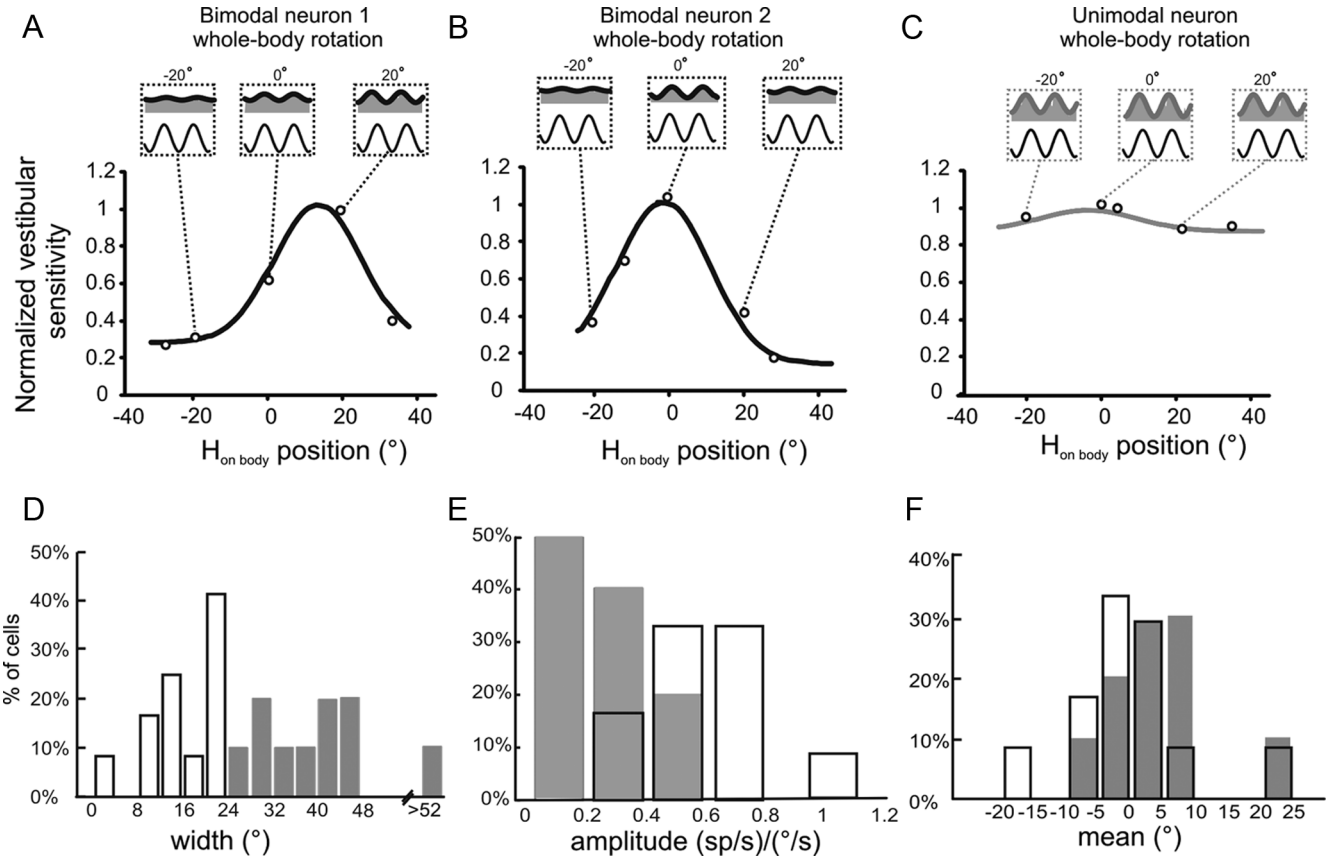

Figure 5. Vestibular sensitivity tuning in response to static head-on-body position changes. Top, Tuning curves for two bimodal neurons (***A***, ***B***) and one unimodal neuron (***C***). Vestibular sensitivity was measured during whole-body rotation with the head oriented at different positions relative to the body (shown in insets). Note that bimodal neurons, but not unimodal neurons, show changes in response at different head-on-body positions. Bottom, Distributions of the widths (***D***), amplitudes (***E***), and means (***F***) of turning curves (respectively) for unimodal (filled bars; $n = 12$) and bimodal (empty bars; $n = 10$) neurons. The average widths and amplitudes of the tuning curves were significantly different for unimodal and bimodal neurons; however, the average means of the tuning curves were not different and were centered on 0°.

correlation coefficients of the vestibular and summation models against each other. Note that the dashed lines correspond to a 0.01 level of significance. Thus, neurons in the top part of the graph represent neurons better fit by the summation model and those in the lower part neurons better fit by the vestibular model. Neurons that fall between the dashed lines represent neurons were equally well fit by both models. Bimodal neuron responses (empty diamonds) were better predicted by the summation model. In contrast the majority of unimodal neurons (13/15) fall between the two diagonal dashed lines, indicating that both models fit neuronal responses equally well. This is what we expected for the two different cell types because bimodal neurons carry both vestibular and proprioceptive sensitivities and therefore their responses should not reflect only vestibular information. In contrast, since unimodal neurons do not respond to proprioceptive stimulation during body-under-head rotation, both models should fit their responses equally well. Next, we compared on a neuron-by-neuron basis and estimated and predicted head-on-body rotation gains (Fig. 4*B*) and phases (Fig. 4*C*) for all the neurons in our sample. Estimated and predicted velocity sensitivities and phases were comparable (Fig. 4*B*,*C*) ($R^2 = 0.96$ and 0.51 for sensitivity and phase, respectively). The similarity between values is shown by the slope of the line fits to the data which were not different from 1 [$p = 0.45$ and 0.14 for gain (Fig. 4*B*) and phase (Fig. 4*C*), respectively], further confirming that the summation model provided a very good estimate of the gain of the responses during combined stimulation.

Influence of head position on single-neuron vestibular responses

Previous studies in the rostral FN have shown that some neurons encode vestibular signals in a body reference frame (Kleine et al., 2004; Shaikh et al. 2004), demonstrating that a reference frame transformation of vestibular signals from head to body centered has occurred. The mechanisms that underlie reference frame transformations are thought to require nonlinear interactions between sensory (e.g., vestibular) and postural (e.g., neck position) signals (for review, see Pouget et al., 2002). Thus, we next addressed the following question: Is the integration of vestibular and proprioceptive information at the level of the rostral FN linear? To address this, we determined whether the responses of unimodal and bimodal neurons were differentially affected by static changes in head-on-body position. Specifically, we measured neuronal responses to whole-body rotation applied with the head positioned at orientations ranging from −20 (left) to +20° (right) relative to the body. Figure 5 illustrates the approach that was used for these measurements. Bimodal neurons showed marked changes in vestibular sensitivity (Fig. 5*A*,*B*; insets show example responses at −20, 0, and 20° head-on-body positions) to changes in head-on-body position. In contrast, unimodal neurons showed little change in sensitivity at different head-on-body positions (Fig. 5*C*). The example bimodal neurons in Figure 5, *A* and *B*, were typical in that their tuning was well described by a Gaussian function (VAF = 0.81 ± 0.15 for our sample of neurons). The two example neurons showed bandpass tuning for

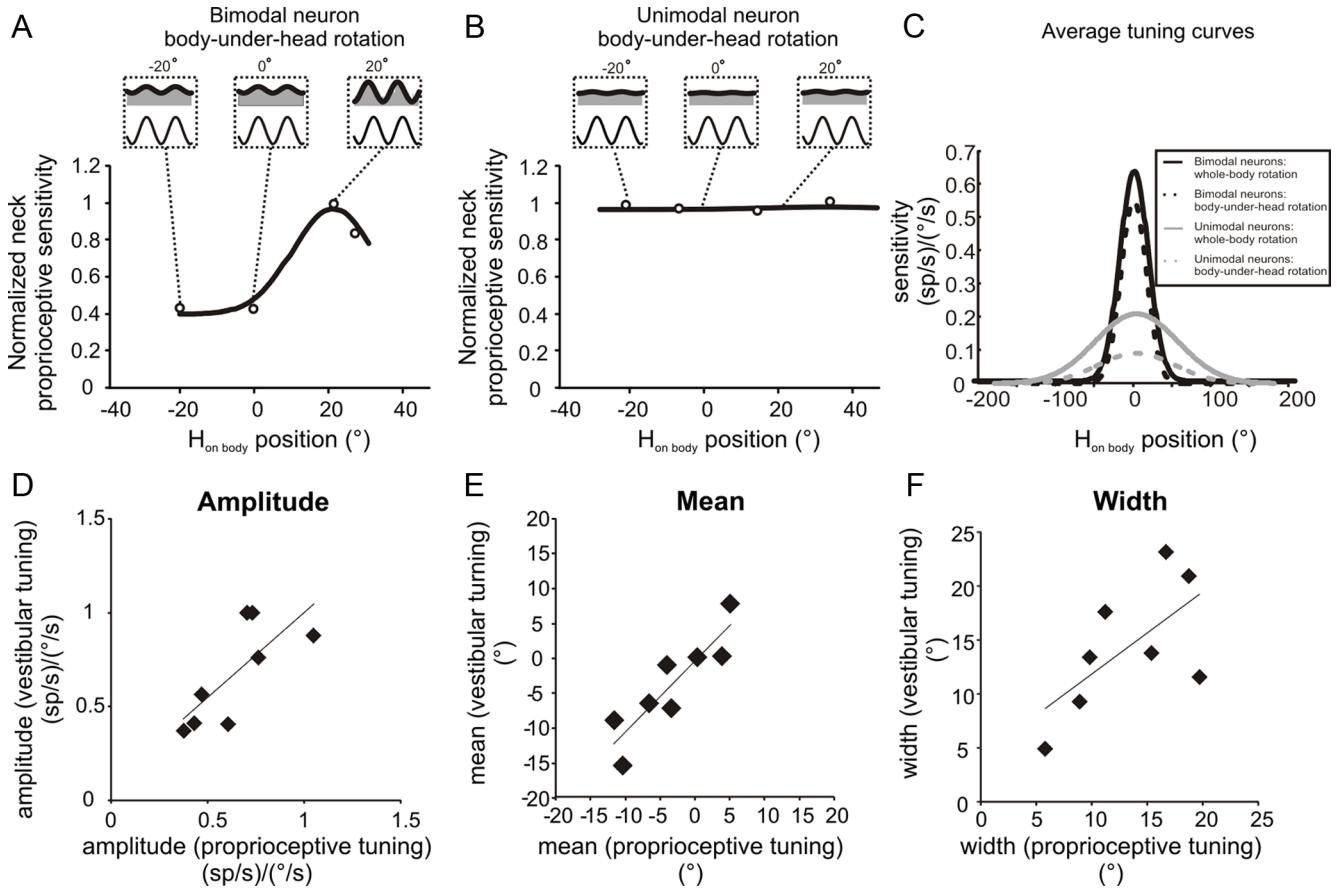

Figure 6. Neck proprioceptive sensitivity tuning in response to static head-on-body position changes. Top, Tuning curves for a bimodal neuron (***A***) and a unimodal neuron (***B***). Neck sensitivity was measured during body-under-head rotations with the head initially at various positions relative to the body (shown in insets). Curves were fit from one neuron's responses to rotations at different head-on-body positions. ***C***, Average tuning curves for bimodal and unimodal neurons for different neck positions to vestibular and neck proprioceptive stimulation. Bottom, Scatter plots of amplitudes (***D***), means (***E***), and widths (***F***) of vestibular and neck stimulation tuning curves for bimodal neurons ($n = 8$).

head orientations of 16 and −1°, respectively. Whereas the responses of unimodal neurons could also be fit using a Gaussian function (VAF = 0.41 ± 0.11), the example neuron in Figure 5*C* was tuned for head-centered rotations, and the depth of tuning was considerably less than that observed for bimodal neurons.

We analyzed the distributions of tuning width (Fig. 5*D*), amplitude (Fig. 5*E*), and mean (Fig. 5*F*) provided by the best Gaussian fit for our population of neurons. The empty bars denote bimodal neurons, whereas the filled bars show the unimodal neurons. First, bimodal neurons were more narrowly tuned than were unimodal neurons. The mean tuning widths for bimodal and unimodal neurons were 16 and 53°, respectively (Fig. 5*D*) ($p < 0.05$). Second, bimodal neurons showed more substantial modulation of their rotational responses as a result of changes in head orientation. The average amplitude of the tuning curves for bimodal versus unimodal neurons (Fig. 5*E*) was 0.63 versus 0.22 (sp/s)/(°/s) ($p < 0.05$), indicating significantly stronger tuning in bimodal than in unimodal neurons. Finally, there was no difference in the mean of the tuning curve between unimodal neurons and bimodal neurons (Fig. 5*F*) ($p = 0.40$). The tuning curves for the entire sample of tested neurons are shown in supplemental Figure 1, *A* and *B*, available at www.jneurosci.org as supplemental material.

Influence of head position on neuronal sensitivities to neck stimulation

In everyday life, for example, during active head-on-body movements, the activation of vestibular receptors is accompanied by simultaneous dynamic stimulation of neck proprioceptors. To determine whether the processing of dynamic neck-related inputs is similarly affected by head-on-body position, the head was initially positioned at a range of orientations ranging from −20° (left) to +20° (right). We then measured neuronal responses during passive body rotation (beneath an earth-fixed head). As can be seen in Figure 6, bimodal neurons showed marked changes in neck sensitivity (Fig. 6*A*), whereas unimodal neurons showed little change in sensitivity at different head-on-body positions (Fig. 6*B*).

A comparison of the tuning of neck and vestibular responses over the population of bimodal neurons revealed that neuronal sensitivities to both inputs were similarly affected by head orientation (Fig. 6*C*). For this analysis, we calculated the population tuning curve by aligning the peak of each individual neuron's tuning curve with zero and averaging the resultant curves. Notably, for both groups of neurons, the average tunings of vestibular- and neck-related responses were comparable (mean tuning widths were 16 and 13°, respectively, for bimodal neurons and 53 and 42° for unimodal neurons). In addition, tuning amplitudes of neck- and vestibular-related responses of bimodal neurons were significantly greater than those of unimodal neurons (for both, $p < 0.05$).

Next, we considered the correlation between properties of the vestibular and neck tuning curves of the bimodal neurons at the level of individual cells. The summary of this analysis is shown in Figure 6*D–F*. We compared the amplitudes, means,

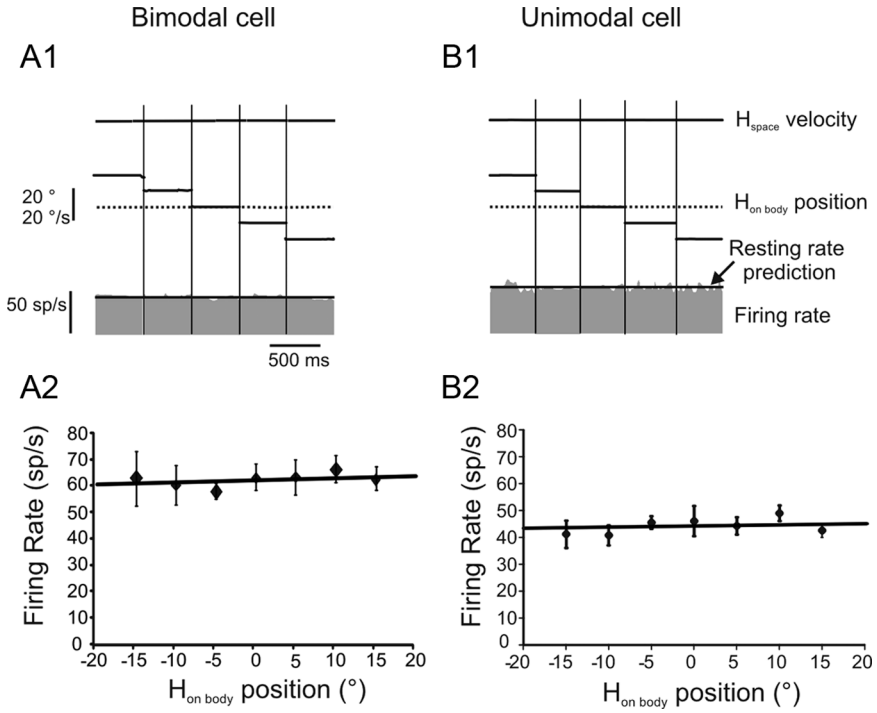

Figure 7. Static neck position sensitivity. Top, Firing rate of the two example neurons (***A1***, ***B1***; same neurons as those shown in Fig. 1) recorded with the head statically shifted to different positions relative to the body. Note that only time intervals during which the head and body are stable in space are displayed and so time is discontinuous between each vertical line. Bottom, Average firing rate of the bimodal (***A2***) and unimodal (***B2***) neurons at different positions (binned in 5° intervals) does not change with neck position; error bars represent ±SE.

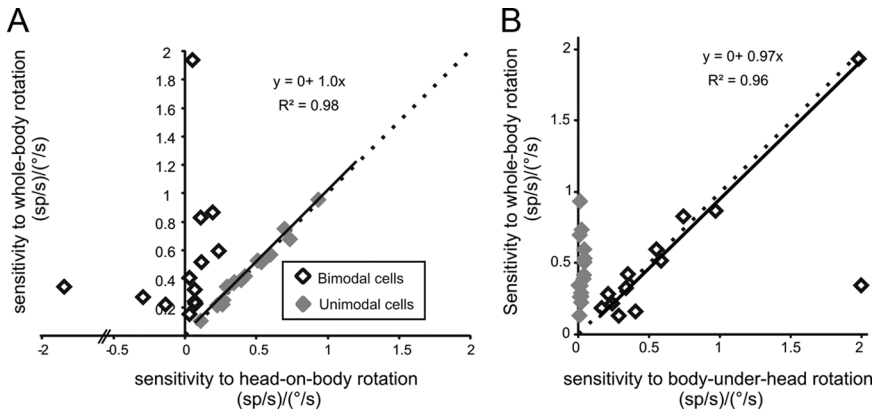

Figure 8. Rostral FN neurons encode motion of the head or of the body. ***A***, Comparison of sensitivities to head-on-body rotation and whole-body rotation for both unimodal (filled diamonds) and bimodal neurons (empty diamonds). In both these paradigms the head is moving relative to space. Note that all filled symbols (unimodal neurons) fall on the unity line (dotted line), suggesting that these neurons encode motion of the head. The black line shows the regression line fit through unimodal neuron data. ***B***, Comparison of sensitivities to body-under-head rotation and whole-body rotation for both unimodal (filled diamonds) and bimodal (empty diamonds) neurons. In both these paradigms the body is moving relative to space. Note that all empty symbols (bimodal neurons) fall on the unity line (dotted line), suggesting that these neurons encode motion of the body. The black line shows the regression line fit through bimodal neuron data.

and widths of the vestibular and neck proprioceptive tuning curves of bimodal neurons. First, there was a positive relationship between the tuning strength (amplitude) of the vestibular and neck proprioceptive responses of bimodal neurons (Fig. 6*D*) ($R^2 = 0.55$; $p < 0.05$). In addition, we found a strong correlation between the mean values (i.e., position of maximum sensitivity) of the vestibular and neck proprioceptive tuning curves (mean) (Fig. 6*E*) ($R^2 = 0.79$; $p < 0.05$). Last, as shown in Figure 6*F*, the widths of the tuning curves for two sensory inputs were also weakly correlated, although this correlation did not reach statistical significance ($R^2 = 0.40$; $p = 0.1$). The significance of these correlations will be addressed in the Discussion.

Influence of static changes in head position on bimodal neuron responses

In response to dynamic neck stimulation produced by head-on-body rotations, the modulations of both unimodal and bimodal neurons were well predicted by the sum of a given neuron's sensitivities to vestibular and proprioceptive stimulation measured when each stimulus was delivered separately (Fig. 3). Moreover, in response to static changes in head orientation, the magnitude of vestibular (Fig. 5) and neck (Fig. 6) sensitivities of bimodal neurons varied as a function of static head orientation. However, in contrast to the dynamic stimulation condition, neck-related responses generated during static changes in head orientation did not simply sum linearly with the applied vestibular stimulation. This can be appreciated by the results shown in Figure 7. Neuronal responses were recorded in the absence of vestibular stimulation during intervals in which the head was systematically rotated relative to the body over a range of ±20° in 5° steps. The example neuron shown in Figure 7*A1* was representative of the bimodal neurons in our sample. Whereas this neuron responded vigorously to sinusoidal rotation of the body under a fixed head (Fig. 3*B*), it was unresponsive to different static positions of the head relative to the body (Fig. 7*A2*) ($p = 0.52$). Notably, its firing rate remained constant and identical to its spontaneous discharge rate measured with the head centered on the body (Fig. 7*A1* prediction, thick trace). Similar results were obtained for our sample of unimodal neurons (Fig. 7*B1*,*B2*) ($p = 0.71$). Thus, the interaction between vestibular responses and head-on-body position information that underlies the tuning shown in Figure 5 is inherently nonlinear. The implications of these findings are further considered in the Discussion.

What signal do neurons encode during self-motion?

Previous studies have suggested that vestibular–somatosensory interactions in the rostral FN implement a coordinate transformation to estimate motion of the body through space (Kleine et al., 2004; Shaikh et al., 2004). These results led to the proposal that neurons in the rostral FN encode the motion of the body rather than the head. However, because the head and body were not moved independently of each other, the question of what

signal is encoded during self-motion was never explicitly addressed.

In the present study, we compared neuronal responses during motion of the head versus body to directly address this question. First, consider the case in which a given neuron encoded head motion—one would expect that it should have the same sensitivity to head motion regardless of whether the head and body move together in space (i.e., whole-body rotation) or the head was rotated on a stationary body (i.e., head-on-body rotation). Indeed, as can be seen in Figure 8*A*, the responses of unimodal neurons were consistent with this prediction; their sensitivities in these two conditions were similar (slope = 1.0; $R^2 = 0.98$). In contrast, data from bimodal neurons fall above the unity line, indicating that they do not respond similarly in these two conditions and thus do not encode head motion (Fig. 8*A*). Second, consider the case in which a given neuron encoded motion of the body—one would expect that it should have the same sensitivity to body motion regardless of whether the head and body move together in space (i.e., whole-body rotation) or the body was rotated beneath a stationary head (i.e., body-under-head rotation). Notably, the responses of our population of bimodal neurons were consistent with this prediction. As is shown in Figure 8*B*, the sensitivities of individual neurons were similar in these two conditions (slope = 0.97; $R^2 = 0.96$), whereas those of the unimodal neurons were not. Together, our results suggest that the primate cerebellum encodes self-motion using two different populations of neurons; unimodal neurons that encode motion of the head in space, and bimodal neurons that encode body motion.

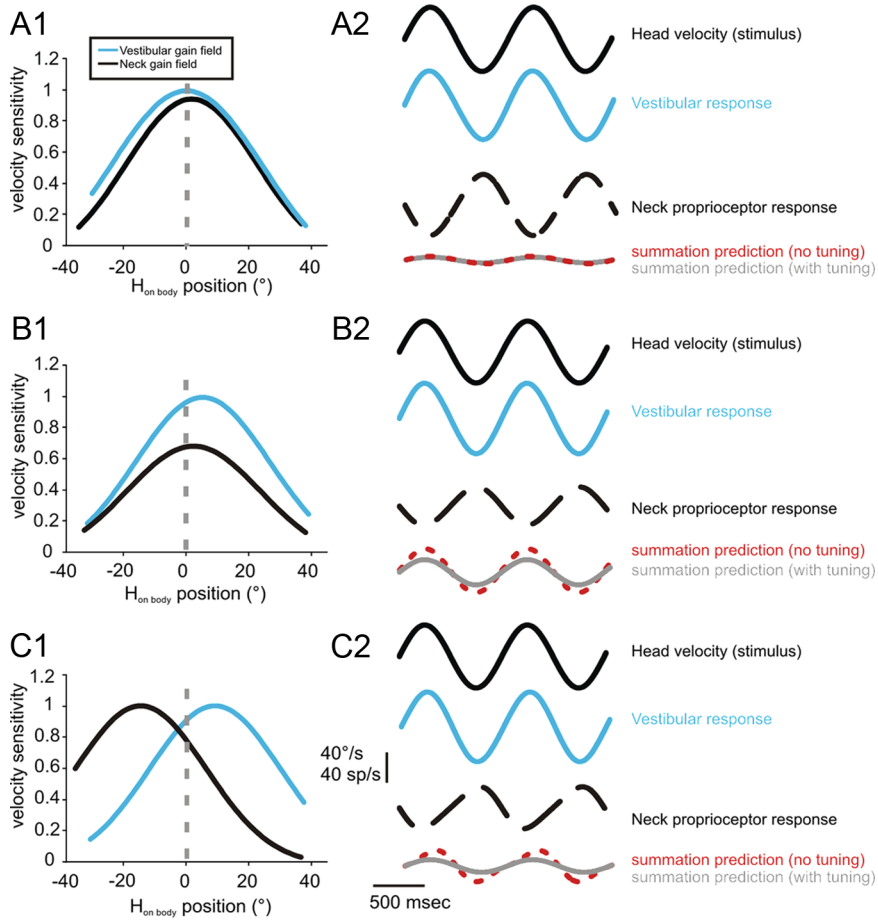

Figure 9. Bimodal neurons have tuning curves for vestibular and neck proprioceptive inputs that are similar. Left, Tuning curves for hypothetical bimodal neurons with neck-position-dependant responses to vestibular (blue curve) and neck (black curve) inputs that are similar (***A1***), have different amplitudes (***B1***), or have different mean values (***C1***). Right, Simulation of vestibular (blue line) and neck (black dashed line) responses as well as predicted combined response (summation prediction) to head-on-body stimulation with (red dotted line) and without (gray line) tuning related to head-on-body position of vestibular and neck inputs for the hypothetical neurons. Notice that modulation is similar when there is no tuning (red dashed line) and when there is tuning (gray line) when the tuning curves are similar (***A2***) but not when the tuning is dissimilar (***B2***, ***C2***). (Summation prediction without tuning is calculated based on sensitivities at the 0° head-on-body position, denoted by the gray dashed line on the left of the figure).

Discussion

These results show that body motion is encoded by a distinct population of neurons in the rostral FN, an area of the cerebellum that receives projections from the vestibular nuclei (Furuya et al., 1975) as well as proprioceptive inputs from the central cervical and external cuneate nuclei (Somana and Walberg, 1980; Xiong and Matsushita, 2001). We found that approximately half of our neurons encoded motion of the body, whereas the other half encoded motion of the head like neurons in the vestibular nuclei. Notably, neurons encoding body motion were characterized by the convergence of vestibular and proprioceptive signals and were consequently classified as bimodal neurons. In contrast, those encoding head motion were sensitive only to vestibular inputs. Interestingly, the vestibular and proprioceptive responses of bimodal neurons showed comparable tuning (e.g., strength and location of maximal response) that varied as a function of head-on-body position. As shown below, this similarity in tuning underlies the ability of rostral FN neurons to robustly encode body motion. We suggest that the neurons that encode body motion (i.e., bimodal neurons) are likely to be the same neurons that have been shown to encode motion in a body-referenced coordinate frame (Kleine et al., 2004; Shaikh et al., 2004), since the accurate encoding of body motion likely requires vestibular signals to be transformed from a head- to a body-centered reference frame.

Fastigial neurons and the encoding of motion

Human subjects perceive rotation of the body with a velocity threshold of ~1°/s (Mergner et al., 1981, 1983, 1991). The integration of vestibular (i.e., head-in-space) information with neck proprioceptive inputs (i.e., head-on-body information) is required for the computation of body motion (Mergner et al., 1981, 1983; Blouin et al., 1995). In turn, this integration of vestibular and neck proprioceptive information is vital for accurate control of posture (Nashner and Wolfson, 1974; Tokita et al., 1989; Kennedy and Inglis, 2002; Hlavacka and Njiokiktjien, 1985; Fransson et al., 2000) and voluntary behaviors such as pointing during self-motion (Mergner et al., 1992; Maurer et al., 1997).

Although there is consensus that the brain computes its estimate of body motion based on the convergence of vestibular and proprioceptive signals, before this study the neural correlate of

body motion had not been identified. Neurons in the vestibular nerve and nuclei of the rhesus monkey encode motion of the head during passive motion (Roy and Cullen, 2001; Cullen and Minor, 2002), despite early vestibular–neck convergence in sensory processing (Boyle and Pompeiano, 1981; Anastasopoulos and Mergner, 1982; Wilson et al., 1990, 1991). The significant convergence of vestibular and proprioceptive inputs within the next stage of processing in the rostral FN nucleus of the cerebellum (Furuya et al., 1975; Wilson et al., 1978; Matsushita and Tanami, 1987; Matsushita and Xiong, 2001) make this area a likely candidate for encoding body motion. Indeed, given that the rostral FN constitutes a major output of the anterior vermis (Verburgh et al., 1989) and nodulus/uvula (Voogd et al., 1996), both of which have been implicated in vestibular–proprioceptive interactions for limb and postural control, our findings suggest that the body motion signals encoded by rostral FN play an important role in the production of accurate motor behaviors. Consistent with this proposal, a recent preliminary report has shown that patients with damage to these structures do not exhibit the systematic changes in body sway that are characteristic of normal subjects when head-on-body position is altered during galvanic stimulation (Kammermeier et al., 2007). Additionally, the rostral FN sends ascending projections to the posterolateral ventral nucleus of the thalamus (Sugimoto et al., 1981; Asanuma et al., 1983), which could potentially provide an estimate of body motion to higher-order structures for the perception of self-motion and computation of spatial orientation.

The fastigial nucleus and reference frame transformations

To produce accurate motor control and sensory perception, it is often necessary to combine vestibular signals with other sensory information to transform the original sensory input from its native reference frame into another that is relevant to ongoing behavior. Vestibular information is first encoded in a head reference frame because the sensors are located in the head. However, when head and body coordinate systems are systematically dissociated, some rostral FN neurons encode motion in a reference frame fixed relative to body rather than head (Kleine et al., 2004; Shaikh et al., 2004). This raises the question of how the sensory convergence observed in the present study corresponds to the transformation of motion from a head- to body-centered reference frame in the rostral FN?

A common feature of theoretical models of reference frame transformations is that responses to sensory inputs (e.g., proprioceptive and/or vestibular information) are modulated by a postural signal (e.g., head-on-body position) (Pouget and Snyder, 2000). These nonlinear interactions can generally take two forms. On one hand, studies have shown that nonlinear interactions between sensory responses and postural cues can result in the amplitude of the directional tuning curve of a neuron being scaled based on the posture (Zipser and Andersen, 1988); this is commonly referred to as a gain field (Andersen and Mountcastle, 1983). On the other hand, the interaction can take the form of a shift in tuning curve without changing the amplitude. The latter has been previously observed in the rostral FN, in which some neurons have tuning curves where the peak modulation remains aligned with the body, despite changing vestibular inputs (Kleine et al., 2004; Shaikh et al., 2004). Alternatively, both types of interactions might be present, as is seen in ventral intraparietal area (Avillac et al., 2005). Although our experimental paradigms do not allow us to distinguish between these possibilities, the nonlinear interactions we observe between neck position and vestibular signals suggest that bimodal but not unimodal neurons are involved in transforming vestibular signals from a head- to a body-centered reference frame.

To date, few studies have explicitly compared the nonlinear processing of two different sensory inputs as a function of a postural cue for the same neuronal population (Avillac et al., 2005; Fetsch et al., 2007). When we compared vestibular and proprioceptive processing as a function of head orientation in individual bimodal neurons, we found that the widths, means, and amplitudes of tuning curves were well correlated. This finding is significant—if this correlation did not exist it would be difficult to reconcile our finding that vestibular and neck inputs sum linearly during combined stimulation (Fig. 4*B*) with the observed nonlinear processing in which head-on-body position modulates the gain of vestibular and dynamic neck proprioceptive responses. To appreciate this point, consider a hypothetical neuron for which the tuning curves of both sensory inputs are comparable (Fig. 9*A1*) versus two others for which there are marked differences in relative strength (Fig. 9*B1*) or direction of tuning (Fig. 9*C1*). During everyday life, vestibular and proprioceptive inputs would be antagonistic, since the motion of the head relative to space (i.e., vestibular stimulation) results in an equal and opposite motion of the body relative to the head (i.e., proprioceptive stimulation). Thus, in the case of the hypothetical neuron with overlapping tuning curves, the effect of head position is effectively cancelled (Fig. 9*A2*, compare vestibular neck proprioceptive inputs). In contrast, when the tuning curves of both sensory inputs are dissimilar, this is not the case (Fig. 9*B2*,*C2*); the vestibular and neck sensitivities change as a function of head-on-body position but do not cancel out when they are combined. Thus, the responses of bimodal neurons sum linearly during combined stimulation because they are similarly tuned to both sensory inputs. In this way, rostral FN neurons robustly encode motion of the body, although their sensory processing is characterized by nonlinear operations. The relationship between the nonlinear interactions observed in our study and those which are thought to underlie the transformation of vestibular inputs from a head- to a body-centered reference frame are still not understood and require further investigation.

Rostral fastigial nucleus during voluntary movements

Thus far, all the experiments we have considered have used passively applied movements exclusively. However, we know that the vestibular nucleus, which is reciprocally connected to the rostral FN (Shimazu and Smith, 1971; Furuya et al., 1975), differentially processes vestibular signals arising from passively applied and actively generated movements (Roy and Cullen, 2001, 2004; Cullen and Minor, 2002; Jamali et al., 2009). Specifically, during active movements, vestibular-only neurons show reduced sensitivity to vestibular stimuli. If body motion is indeed computed from a convergence of vestibular and neck inputs and vestibular information is reduced during active movements, how is body motion computed during voluntary motion? One possibility is that vestibular-driven responses are not attenuated in the rostral FN during active movements. Alternatively, additional signals available during voluntary movements, such as efference copy or higher-order cortical signals related to the intention to move, could be used to keep track of our body motion in space. Further experiments are needed to determine the role of the rostral FN during voluntary movements.

References

Anastasopoulos D, Mergner T (1982) Canal-neck interaction in vestibular nuclear neurons of the cat. Exp Brain Res 46:269–280.

Andersen RA, Mountcastle VB (1983) The influence of the angle of gaze upon the excitability of the light-sensitive neurons of the posterior parietal cortex. J Neurosci 3:532–548.

Angelaki DE, Shaikh AG, Green AM, Dickman JD (2004) Neurons compute internal models of the physical laws of motion. Nature 430:560–564.

Asanuma C, Thach WT, Jones EG (1983) Distribution of cerebellar terminations and their relation to other afferent terminations in the ventral lateral thalamic region of the monkey. Brain Res 286:237–265.

Avillac M, Denève S, Olivier E, Pouget A, Duhamel JR (2005) Reference frames for representing visual and tactile locations in parietal cortex. Nat Neurosci 8:941–949.

Blouin J, Vercher JL, Gauthier GM, Paillard J, Bard C, Lamarre Y (1995) Perception of passive whole-body rotations in the absence of neck and body proprioception. J Neurophysiol 74:2216–2219.

Boyle R, Pompeiano O (1981) Convergence and interaction of neck and macular vestibular inputs on vestibulospinal neurons. J Neurophysiol 45:852–868.

Cullen KE, McCrea RA (1993) Firing behavior of brain stem neurons during voluntary cancellation of the horizontal vestibuloocular reflex. I. Secondary vestibular neurons. J Neurophysiol 70:828–843.

Cullen KE, Minor LB (2002) Semicircular canal afferents similarly encode active and passive head-on-body rotations: implications for the role of vestibular efference. J Neurosci 22:RC226.

Cullen KE, Rey CG, Guitton D, Galiana HL (1996) The use of system identification techniques in the analysis of oculomotor burst neuron spike train dynamics. J Comput Neurosci 3:347–368.

Cullen KE, Roy JE, Sylvestre PA (2001) Signal processing by vestibular nuclei neurons is dependent on the current behavioral goal. Ann N Y Acad Sci 942:345–363.

Fetsch CR, Wang S, Gu Y, Deangelis GC, Angelaki DE (2007) Spatial reference frames of visual, vestibular, and multimodal heading signals in the dorsal subdivision of the medial superior temporal area. J Neurosci 27:700–712.

Fransson PA, Karlberg M, Sterner T, Magnusson M (2000) Direction of galvanically-induced vestibulo-postural responses during active and passive neck torsion. Acta Otolaryngol 120:500–503.

Fuchs AF, Robinson DA (1966) A method for measuring horizontal and vertical eye movement chronically in the monkey. J Appl Physiol 21:1068–1070.

Furuya N, Kawano K, Shimazu H (1975) Functional organization of vestibulofastigial projection in the horizontal semicircular canal system in the cat. Exp Brain Res 24:75–87.

Gardner EP, Fuchs AF (1975) Single-unit responses to natural vestibular stimuli and eye movements in deep cerebellar nuclei of the alert rhesus monkey. J Neurophysiol 38:627–649.

Hayes AV, Richmond BJ, Optican LM (1982) A UNIX-based multiple process system for real-time data acquisition and control. In: Western Electronic Show and Conference Proceedings, Vol 2, pp 1–10. New York: Institute of Electrical and Electronics Engineers.

Hlavacka F, Njiokiktjien C (1985) Postural responses evoked by sinusoidal galvanic stimulation of the labyrinth. Influence of head position. Acta Otolaryngol 99:107–112.

Jamali M, Sadeghi SG, Cullen KE (2009) Response of vestibular nerve afferents innervating utricle and saccule during passive and active translations. J Neurophysiol 101:141–149.

Judge SJ, Richmond BJ, Chu FC (1980) Implantation of magnetic search coils for measurement of eye position: an improved method. Vision Res 20:535–538.

Kammermeier S, Kleine JF, Büttner U (2007) Impaired vestibulo-proprioceptive interaction in cerebellar patients. Soc Neurosci Abstr 33:512.13/RR17.

Kennedy PM, Inglis JT (2002) Interaction effects of galvanic vestibular stimulation and head position on the soleus H reflex in humans. Clin Neurophysiol 113:1709–1714.

Kleine JF, Guan Y, Kipiani E, Glonti L, Hoshi M, Büttner U (2004) Trunk position influences vestibular responses of fastigial nucleus neurons in the alert monkey. J Neurophysiol 91:2090–2100.

Matsushita M, Tanami T (1987) Spinocerebellar projections from the central cervical nucleus in the cat, as studied by anterograde transport of wheat germ agglutinin-horseradish peroxidase. J Comp Neurol 266:376–397.

Matsushita M, Xiong G (2001) Uncrossed and crossed projections from the upper cervical spinal cord to the cerebellar nuclei in the rat, studied by anterograde axonal tracing. J Comp Neurol 432:101–118.

Maurer C, Kimmig H, Trefzer A, Mergner T (1997) Visual object localization through vestibular and neck inputs. 1: Localization with respect to space and relative to the head and trunk mid-sagittal planes. J Vestib Res 7:119–135.

McCluskey MK, Cullen KE (2007) Eye, head, and body coordination during large gaze shifts in rhesus monkeys: movement kinematics and the influence of posture. J Neurophysiol 97:2976–2991.

McCrea RA, Gdowski GT, Boyle R, Belton T (1999) Firing behavior of vestibular neurons during active and passive head movements: vestibulospinal and other non-eye-movement related neurons. J Neurophysiol 82:416–428.

Mergner T, Anastasopoulos D, Becker W, Deecke L (1981) Discrimination between trunk and head rotation; a study comparing neuronal data from the cat with human psychophysics. Acta Psychol (Amst) 48:291–301.

Mergner T, Nardi GL, Becker W, Deecke L (1983) The role of canal-neck interaction for the perception of horizontal trunk and head rotation. Exp Brain Res 49:198–208.

Mergner T, Siebold C, Schweigart G, Becker W (1991) Human perception of horizontal trunk and head rotation in space during vestibular and neck stimulation. Exp Brain Res 85:389–404.

Mergner T, Rottler G, Kimmig H, Becker W (1992) Role of vestibular and neck inputs for the perception of object motion in space. Exp Brain Res 89:655–668.

Nashner LM, Wolfson P (1974) Influence of head position and proprioceptive cues on short latency postural reflexes evoked by galvanic stimulation of the human labyrinth. Brain Res 67:255–268.

Pouget A, Snyder LH (2000) Computational approaches to sensorimotor transformations. Nat Neurosci [Suppl] 3:1192–1198.

Pouget A, Deneve S, Duhamel JR (2002) A computational perspective on the neural basis of multisensory spatial representations. Nat Rev Neurosci 3:741–747.

Roy JE, Cullen KE (1998) A neural correlate for vestibulo-ocular reflex suppression during voluntary eye-head gaze shifts. Nat Neurosci 1:404–410.

Roy JE, Cullen KE (2001) Selective processing of vestibular reafference during self-generated head motion. J Neurosci 21:2131–2142.

Roy JE, Cullen KE (2004) Dissociating self-generated from passively applied head motion: neural mechanisms in the vestibular nuclei. J Neurosci 24:2102–2111.

Sadeghi SG, Mitchell DE, Cullen KE (2009) Different neural strategies for multimodal integration: comparison of two macaque monkey species. Exp Brain Res 195:45–57.

Scudder CA, Fuchs AF (1992) Physiological and behavioral identification of vestibular nucleus neurons mediating the horizontal vestibuloocular reflex in trained rhesus monkeys. J Neurophysiol 68:244–264.

Shaikh AG, Meng H, Angelaki DE (2004) Multiple reference frames for motion in the primate cerebellum. J Neurosci 24:4491–4497.

Shaikh AG, Ghasia FF, Dickman JD, Angelaki DE (2005) Properties of cerebellar fastigial neurons during translation, rotation, and eye movements. J Neurophysiol 93:853–863.

Shimazu H, Smith CM (1971) Cerebellar and labyrinthine influences on single vestibular neurons identified by natural stimuli. J Neurophysiol 34:493–508.

Smith MA, Majaj NJ, Movshon JA (2005) Dynamics of motion signaling by neurons in macaque area MT. Nat Neurosci 8:220–228.

Somana R, Walberg F (1980) A re-examination of the cerebellar projections from the gracile, main and external cuneate nuclei in the cat. Brain Res 186:33–42.

Stanojević M (1981) Responses of cerebellar fastigial neurons to neck and macular vestibular inputs. Pflugers Arch 391:267–272.

Sugimoto T, Mizuno N, Itoh K (1981) An autoradiographic study on the terminal distribution of cerebellothalamic fibers in the cat. Brain Res 215:29–47.

Sylvestre PA, Cullen KE (1999) Quantitative analysis of abducens neuron discharge dynamics during saccadic and slow eye movements. J Neurophysiol 82:2612–2632.

Tokita T, Ito Y, Takagi K (1989) Modulation by head and trunk positions of the vestibulo-spinal reflexes evoked by galvanic stimulation of the laby-

rinth. Observations by labyrinthine evoked EMG. Acta Otolaryngol 107:327–332.

Tokita T, Miyata H, Takagi K, Ito Y (1991) Studies on vestibulo-spinal reflexes by examination of labyrinthine-evoked EMGs of lower limbs. Acta Otolaryngol [Suppl] 481:328–332.

Verburgh CA, Kuypers HG, Voogd J, Stevens HP (1989) Spinocerebellar neurons and propriospinal neurons in the cervical spinal cord: a fluorescent double-labeling study in the rat and the cat. Exp Brain Res 75:73–82.

Voogd J, Gerrits NM, Ruigrok TJ (1996) Organization of the vestibulocerebellum. Ann N Y Acad Sci 781:553–579.

Wilson VJ (1991) Vestibulospinal and neck reflexes: interaction in the vestibular nuclei. Arch Ital Biol 129:43–52.

Wilson VJ, Uchino Y, Maunz RA, Susswein A, Fukushima K (1978) Properties and connections of cat fastigiospinal neurons. Exp Brain Res 32:1–17.

Wilson VJ, Yamagata Y, Yates BJ, Schor RH, Nonaka S (1990) Response of vestibular neurons to head rotations in vertical planes. III. Response of vestibulocollic neurons to vestibular and neck stimulation. J Neurophysiol 64:1695–1703.

Xiong G, Matsushita M (2001) Ipsilateral and contralateral projections from upper cervical segments to the vestibular nuclei in the rat. Exp Brain Res 141:204–217.

Zipser D, Andersen RA (1988) A back-propagation programmed network that simulates response properties of a subset of posterior parietal neurons. Nature 331:679–684.